Modification of Jupiter's Stratosphere Three Weeks After the 2009 Impact

Short Title: Jupiter's Stratosphere Three Weeks After 2009 Impact

Kelly E. Fast[1], Theodor Kostiuk[1]
Planetary Systems Laboratory, Code 693
NASA Goddard Space Flight Center
Greenbelt, Maryland 20771

Timothy A. Livengood[1,2]
National Center for Earth and Space Science Education
PO Box 3806, Capitol Heights, MD 20791-3806

Tilak Hewagama[2]
Department of Astronomy, University of Maryland
College Park, Maryland 20742-2421

John Annen[1]
Planetary Systems Laboratory, Code 693
NASA Goddard Space Flight Center
Greenbelt, Maryland 20771

[1] Visiting Astronomer at the Infrared Telescope Facility, which is operated by the University of Hawaii under Cooperative Agreement no. NCC 5-538 with the National Aeronautics and Space Administration, Science Mission Directorate, Planetary Astronomy Program.

[2] Also at Planetary Systems Laboratory, Code 693, NASA Goddard Space Flight Center, Greenbelt, Maryland 20771

Correspondence Address: Kelly E. Fast
Code 693 NASA/GSFC
Greenbelt, MD 20771
Phone: 301-286-7689
Fax: 301-286-1683
E-mail: Kelly.E.Fast@nasa.gov

ABSTRACT

Infrared spectroscopy sensitive to thermal emission from Jupiter's stratosphere reveals effects persisting 23 days after the impact of a body in late July 2009. Measurements obtained on 2009 August 11 UT at the impact latitude of 56°S (planetocentric), using the Goddard Heterodyne Instrument for Planetary Wind and Composition mounted on the NASA Infrared Telescope Facility, reveal increased ethane abundance and the effects of aerosol opacity. An interval of reduced thermal continuum emission at 11.744 μm is measured ~60°–80° towards planetary east of the impact site, estimated to be at 305° longitude (System III). Retrieved stratospheric ethane mole fraction in the near vicinity of the impact site is enhanced by up to ~60% relative to quiescent regions at this latitude. Thermal continuum emission at the impact site, and somewhat west of it, is significantly enhanced in the same spectra that retrieve enhanced ethane mole fraction. Assuming that the enhanced continuum brightness near the impact site results from thermalized aerosol debris blocking contribution from the continuum formed in the upper troposphere and indicating the local temperature, then continuum emission by a haze layer can be approximated by an opaque surface inserted at the 45-60 mbar pressure level in the stratosphere in an unperturbed thermal profile, setting an upper limit on the pressure and therefore a lower limit on the altitude of the top of the impact debris at this time. The reduced continuum brightness east of the impact site can be modeled by an opaque surface near the cold tropopause, which is consistent with a lower altitude of ejecta/impactor-formed opacity or significantly lesser column density of opaque haze material. The physical extent of the observed region of reduced continuum implies a minimum average velocity of 21 m/s transporting material prograde (planetary east) from the impact.

Key words: Jupiter, atmosphere; Impact processes; Infrared observations; Atmospheres, composition; Atmospheres, dynamics

1. INTRODUCTION

The comet Shoemaker-Levy 9 (SL9) impacts on Jupiter in July 1994 appeared then to be a unique opportunity to investigate giant impacts and restorative processes in a strongly perturbed Jovian atmosphere [e.g., Harrington et al. 2004]. On 2009 July 19, A. Wesley in Murrumbateman, Australia discovered a new dark spot in Jupiter's southern hemisphere that closely resembled the SL9 impact sites and that had not been observed on preceding nights [Sánchez-Lavega et al., 2010; Hammel et al., 2010], providing a new opportunity to build on the experience of SL9. We incorporated spectroscopy of the impact site region into Jupiter observations in 2009 August at the NASA Infrared Telescope Facility (IRTF) on Mauna Kea, Hawaii. A significant result of studying the SL9 impacts was the discovery of many after-effects in the planet's stratosphere, such as the injection and photodestruction of tropospheric NH_3 [e.g., Kostiuk et al., 1996; Griffith et al., 1997; Fast et al., 2002], shock-produced H_2O [e.g., Bjoraker et al., 1996], thermal modification [e.g., Lellouch et al. 1995; Orton et al., 1995; Bézard et al. 1997] and aerosol deposition, dispersal, and sedimentation [e.g., West et al., 1995]. The planned observing technique for 2009, sensitive to infrared auroral activity in the polar regions, also was well-suited to investigate the post-impact stratosphere as debris settled and equilibrium chemistry re-established itself. We report here on high-resolution mid-infrared spectroscopy of stratospheric ethane (C_2H_6) at the impact latitude of 56°S (planetocentric), 23 days after impact, finding a modest local enhancement in stratospheric C_2H_6 concentration near the impact site (Fig. 1) and significant changes in continuum emission near and east of the impact site that constrain the vertical distribution of debris and the stratospheric wind speed and direction.

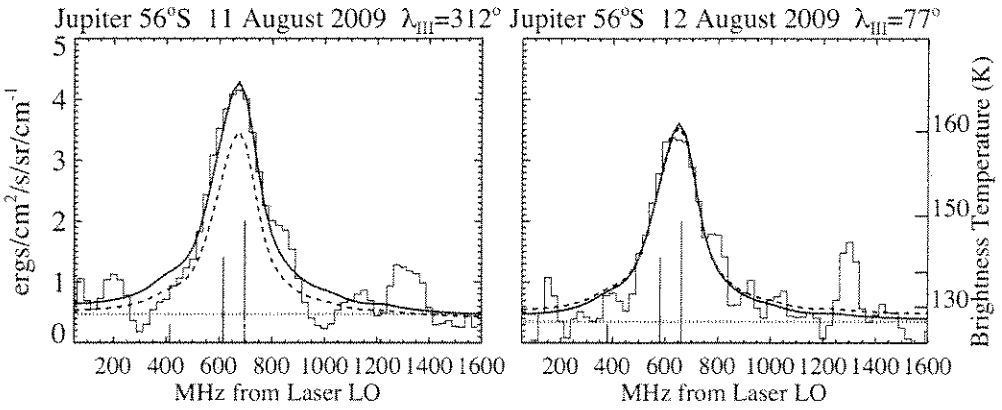

47

48 Approximate location of Figure 1 (see FIGURE CAPTIONS section)

49

50 2. OBSERVATIONS

51 Infrared spectra, targeting the 56° south impact latitude on Jupiter, were acquired on 2009
52 August 11 and 12 (UT) using the NASA Goddard Space Flight Center's Heterodyne Instrument
53 for Planetary Wind And Composition (HIPWAC) at the IRTF (Fig. 2). HIPWAC is a mid-
54 infrared heterodyne spectrometer that obtains very high spectral resolving power ($\lambda/\Delta\lambda>10^6$) by
55 mixing an infrared laser local oscillator with light collected from a target, generating the
56 difference-frequency spectrum at radio frequencies about the local oscillator. For this
57 investigation, a carbon-14 dioxide gas-laser local oscillator provided access to the spectral
58 bandwidth of ±0.0534 cm^{-1} (±1.6 GHz) centered on the $^{14}CO_2$ P18 transition at 851.4895 cm^{-1}
59 (11.744 μm, 25.53 THz). Absolute intensity calibration is provided by a calibrated internal
60 thermal source, the measured reflectivity and transmittance of optical elements, and the
61 transmittance of Earth's atmosphere at the observed airmass and wavelength. Calibration
62 measurements were acquired before, once during, and after the sequence of measurements on
63 August 11 described here. Other instrument performance parameters (e.g., HgCdTe detector bias
64 voltage) showed that instrument performance remained consistent throughout this period.

65 Meteorological data collected by the Canada-France-Hawaii Telescope indicated consistently
66 good conditions (www.cfht.hawaii.edu/cgi-
67 bin/uncgi/elixir/skyprobe.pl?plot&mcal_20090810.png).

68 The spectra were sampled by a discrete 64-channel filter-bank with a resolution of
69 25 MHz (8.3×10^{-4} cm^{-1}). The distribution of power as a function of difference frequency
70 accurately measures true line shapes of spectral features, while high spectral resolving power
71 unambiguously identifies molecular species. Fully-resolved molecular line shapes constrain
72 species abundance and the thermal profile in the region of line formation. The infrared
73 heterodyne technique and the unique features of very high-resolution spectroscopy of planetary
74 atmospheres are described in greater detail by Kostiuk [1994] and by Kostiuk and Mumma
75 [1983].

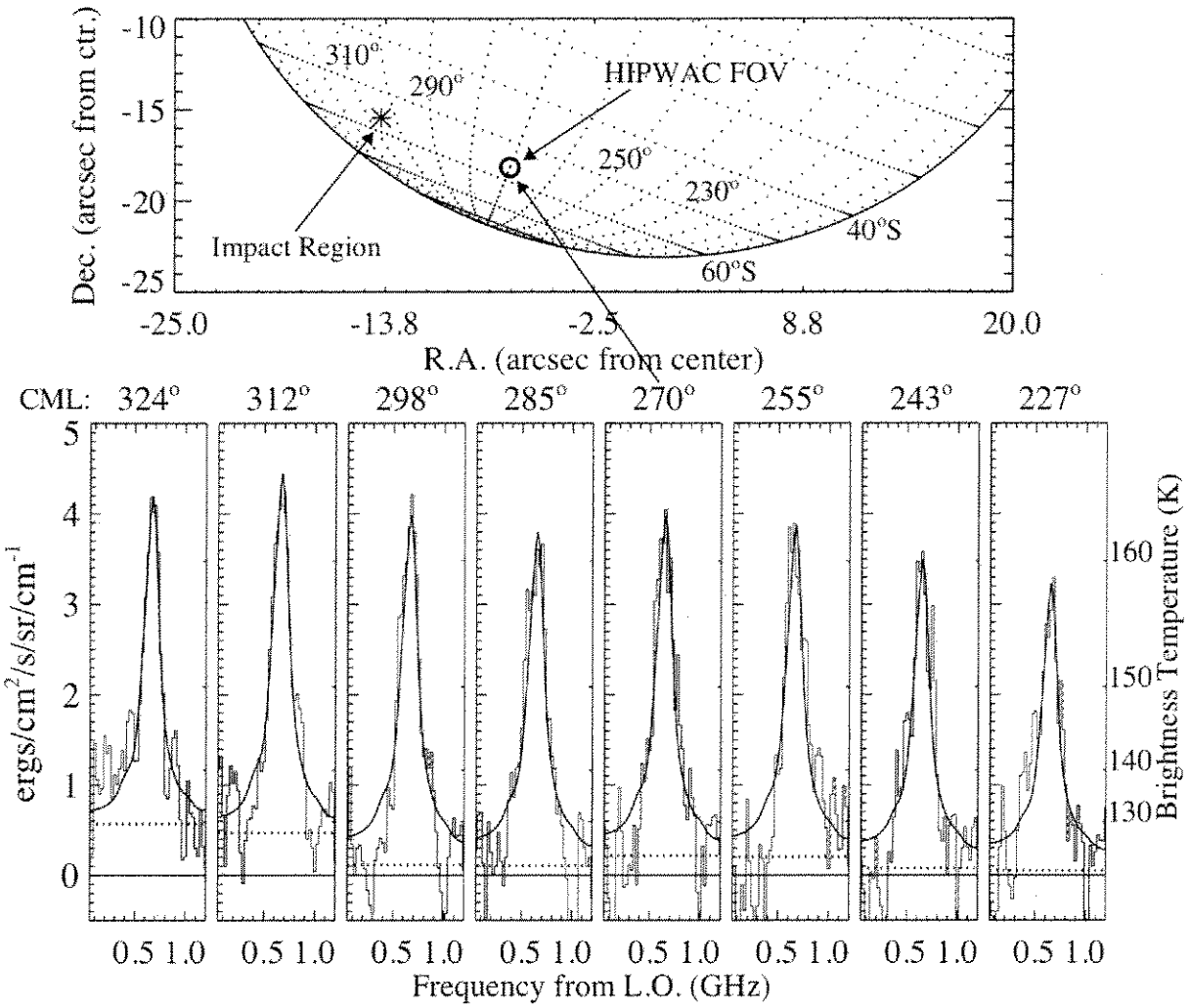

Approximate location of Figure 2 (see FIGURE CAPTIONS section)

HIPWAC's narrow, high-resolution bandpass was configured to detect individual features of ethane (C_2H_6) for the granted polar auroral investigation, therefore ethane served as the target for this unexpected opportunity to investigate a post-impact Jovian stratosphere. Ethane is a stable product of methane (CH_4) photochemistry that is nearly uniformly mixed in Jupiter's stratosphere and is the second-most significant carbon reservoir after methane. Molecular features formed in the positive temperature gradient of a planetary stratosphere appear in emission (Figs. 1 and 2). The principal ethane feature in the measured spectra is a doublet at

~600 MHz, transitions RR(5,11,1) and RR(5,11,3) in the ν_9 band [Atakan et al., 1983; Daunt et al., 1984] at 11.74391 μm rest wavelength (851.5051 cm^{-1}). The HIPWAC field of view (FOV) at this wavelength is ~0.84" full-width at half-maximum (FWHM), nearly diffraction-limited on the 3 m NASA IRTF telescope. The FOV spans ~5° of longitude, centered on the central meridian at the 56°S impact latitude on the 49 arcsecond disk of Jupiter. Spectra were acquired by maintaining the FOV pointing on the central meridian and integrating a sequence of ~4-minute scans while Jupiter's rotation scanned a range of longitude across the FOV. Individual spectral scans have been averaged into overlapping groups (Fig. 2) to provide sufficient signal-to-noise ratio, covering 10°-20° in longitude. The varying Doppler shift due to relative motion of Earth and Jupiter and due to Earth's rotation has been corrected by shifting to a common frequency scale before averaging. Unidentified features in this spectral region at 1300 MHz and at 200 MHz are not instrumental artifacts and are excluded from the present analysis.

The date and time (UT) and central meridian longitude (CML) of the ten spectra extracted from the measurements, as well as the C_2H_6 mole fraction and continuum brightness retrieved from radiative-transfer analysis (described below), are reported in Table 1. All longitudes used in this work are reported in System III Jovimagnetic coordinates (e.g., Russell and Dougherty 2010). The spectral interval near the line peak is displayed in Fig. 2 for the eight spectra nearest the impact site at 305° longitude. One spectrum with high signal-to-noise ratio was acquired at 77° CML on August 12 (Fig. 1). Another spectrum of modest signal-to-noise ratio at 125° CML was acquired on August 11. Both regions are far from the impact site and there is no evidence that they are affected by the impact. The remaining eight spectra are composed of scans acquired on August 11. The peak brightness temperature at line core in the spectrum at 312° CML is greater than the rest (Figs. 1 and 2). Continuum in the spectra east (on

109 Jupiter) of the impact site is depressed relative to the continuum observed at 77° CML, which
110 reflects approximately quiescent conditions at the impact latitude.
111
112 Approximate location of Table 1 (see TABLE section)
113
114 3. RADIATIVE-TRANSFER ANALYSIS
115 Quantitative results from radiative-transfer analysis of the emergent spectra are reported
116 in Table 1. The radiative-transfer techniques employed here are those of Hewagama et al. [2008].
117 Spectral line parameters were derived from direct laboratory measurements targeting ethane
118 features near $^{14}CO_2$ lasing transitions for heterodyne investigations, consistent with Daunt et al.
119 [1984] and Atakan et al. [1983], and nearly identical with recent values from Vander Auwera et
120 al. [2007], which are required to accurately model individual molecular features at infrared
121 heterodyne spectral resolution. A model of the measured ethane emission spectrum is
122 synthesized by combining the model spectrum in many sub-resolution elements, weighted by an
123 approximation to the telescope point-spread function, to simulate the integrated beam detected
124 by the spectrometer. The sub-resolution elements differ in slant angle and in the projected radial
125 velocity due to Jupiter rotation. Finite seeing and tracking uncertainties were incorporated by
126 adjusting the modeled beam width to 1.8" FWHM, blurring the modeled ethane doublet
127 consistent with the measured spectrum. Fitted parameters in the atmospheric model (e.g., ethane
128 mole fraction, temperature, continuum emission, Doppler shift) are iteratively improved to best
129 fit the measured spectrum with the modeled emergent spectrum. Uncertainties are derived from
130 exploring the goodness of fit in the vicinity of the best fit.
131 Similar analysis of infrared heterodyne spectroscopy retrieved an ethane mole fraction of

132 2.8±0.6 ppmv (parts per million by volume) in Jupiter's unperturbed equatorial stratosphere in
133 the 0.2-20 mbar region [Kostiuk et al., 1987, 1989; Livengood et al., 1993], assuming a thermal
134 profile derived from Voyager Infrared Interferometer Spectrometer (IRIS) measurements [Hanel
135 et al., 1979]. A simultaneous fit to ethane mole fraction and stratospheric temperature for the
136 2009 August spectrum with high signal-to-noise ratio at 77° longitude yields mole fraction
137 nearly identical to the quiescent equatorial retrieval. The partially-saturated ethane emission line
138 peak requires a temperature in the 1–10 mbar region, in which the line-center contribution
139 function peaks, that is similar to *Voyager* retrievals near this latitude but a few Kelvin greater
140 than the temperature in profiles derived from more-recent *Cassini* CIRS data [Nixon et al.,
141 2007], from the December 2000 Jupiter flyby. The impact took place during northern Jovian
142 spring, the *Voyager* flybys in autumn, and the *Cassini* flyby in summer. Since there is no
143 seasonal match, neither empirical thermal profile is inherently a better choice. Since the
144 retrieved temperature at 77° longitude corresponds most closely to the *Voyager* profile, we adopt
145 that profile for this investigation in order to minimize free atmospheric parameters. The
146 remaining fitted parameters are a constant-with-height ethane mole fraction profile above the
147 tropopause, the continuum emission brightness, and Doppler shift to account for modest
148 deviations from tracking precisely on Jupiter's central meridian. The contribution to the ethane
149 emission line originates in the 0.2-20 mbar region, with the bulk of the contribution peaking at
150 ~2 mbar.
151 In principle, the fully-resolved ethane line shapes contain information on both mole
152 fraction and temperature in the region of line formation and both parameters could be fitted for
153 each measured spectrum just as for the test fit to the 77° longitude spectrum. In practice, the
154 signal-to-noise ratio in these particular measurements is not sufficient to unambiguously

distinguish between spatial variations in composition *vs.* spatial variations in stratospheric temperature, based on spectroscopic constraints alone. We discount the possibility of spatially variable temperature in the measured spectra for several reasons independent of spectroscopic constraints, holding the temperature profile steady and fitting the ethane mole fraction:

1. Stratospheric thermal decay measured after the much larger SL9 impacts [e.g. Bézard, 1997; Lellouch et al., 1995] and unperturbed temperatures in infrared heterodyne spectroscopy of ammonia, 18 days after a major SL9 impact [Fast et al., 2002], suggest that residual heat from the impact should have dissipated long before three weeks. Other investigations of the August 2009 impact region support thermal decay by three weeks post-impact [Orton et al., 2010; dePater et al., 2010; Fletcher et al., 2010*a,b*].
2. Additional opacity in the stratosphere from impact debris would not heat it, but could conceivably cool it. The stratosphere is heated by solar UV absorption and cooled by infrared radiation. The stratospheric temperature is greater than radiative equilibrium at 5 AU because it radiates inefficiently. Increased opacity could radiate more effectively and thereby cool the stratosphere, but not heat it. There is no evidence for such a thermally-driven decrease in emission by stratospheric ethane.
3. Wave phenomena have been suggested informally as a mechanism for zonal thermal variability in the stratosphere. No prior infrared heterodyne measurement has needed to invoke such an hypothesis under equilibrium conditions. If the variation in ethane emission brightness were due entirely to thermal variations, such as variations that might be indicative of Rossby waves [e.g., Deming et al. 1997; Flasar et al. 2004], temperature increases of over 5 K in the few mbar region where the line peaks form are required to fit the emission, which is high compared to ~1 K variations reported by Deming et al. [1997]. The measured

178 continuum brightness variation is not in the same sense as the ethane emission brightness
179 variation, and the corresponding continuum brightness temperatures vary by over 10 K
180 (Fig. 3). It is possible that an impact initiates a standing wave, which plausibly might not
181 have been observed during the SL9 impacts due to the superposition of so many inputs. The
182 distant spectra at 77° and 125° longitude do not appear consistent with either a local
183 minimum in stratospheric temperature due to a wave of wavenumber 1, or a local maximum
184 due to a wave of wavenumber 2. Without specific evidence, there is no reason to
185 contemplate a more complex waveform.
186 4. There is a strong plausibility argument for compositional perturbations arising and persisting.
187 Jupiter's polar auroral stratosphere, for example, shows evidence of non-equilibrium
188 chemistry due to high-energy particle input [Kim et al., 1985; Kostiuk et al., 1993;
189 Livengood et al., 1993]. Ethane's long photochemical lifetime, of order ~100 years
190 [Gladstone 1983], ensures that dissipation from impact-chemistry is only by transport and
191 diffusion rather than by rapid photochemical destruction.
192
193 4. RESULTS
194 Quantitative radiative-transfer results from fitting each of the spectra of Fig. 2 are
195 reported in Table 1 and displayed in Fig. 3. The retrieved continuum brightness is significantly
196 depressed over a substantial range of longitude to the east (on Jupiter) of the impact site at 305°
197 longitude, and is significantly enhanced in the spectra west of the impact site. The retrieved
198 ethane mole fraction is generally within the generous uncertainty limits of the quiescent value of
199 2.8±0.6 ppmv, but is outside that limit in the two spectra just west of the impact site.
200 Furthermore, the sequence of retrievals east of the impact site shows an increasing trend with

longitude, from a slight depression in retrieved mole fraction farthest from the impact site at 227° longitude up to a peak at 312° longitude (Fig. 1).

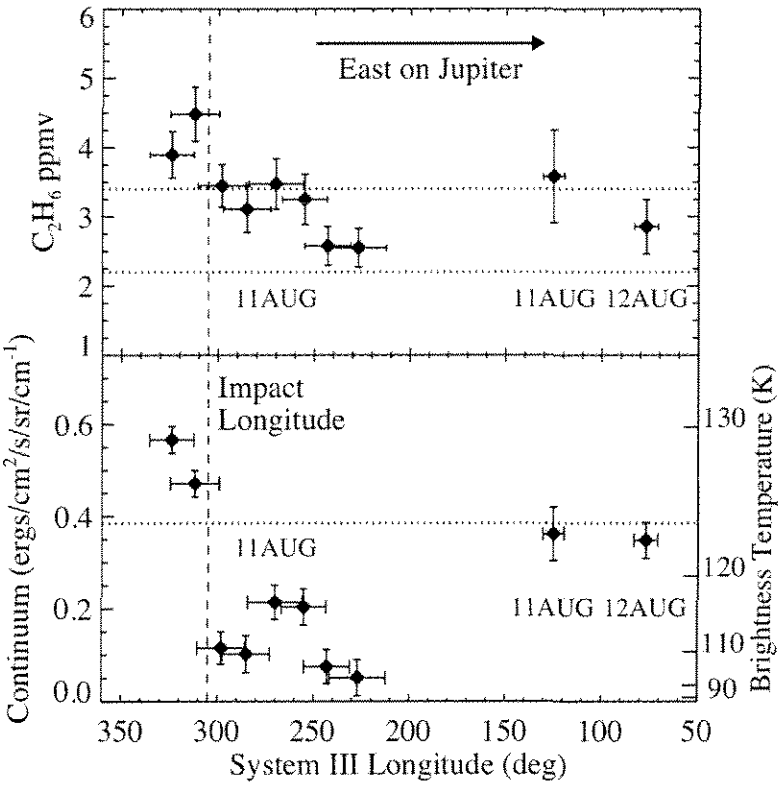

Approximate location of Figure 3 (see FIGURE CAPTIONS section)

The ethane mole fraction of 2.9±0.4 ppmv retrieved from the high signal-to-noise spectrum acquired far from the impact site, at 77° longitude, is consistent with the unperturbed stratosphere and is adopted here as a standard for that condition. The maximum retrieved ethane mole fraction is 4.5±0.4 ppmv at 312° longitude, 60% greater than the retrieval at 77° longitude, with continuum 40% brighter than 77° longitude. The maximum retrieved continuum brightness at 324° longitude, on the other hand, is 60% greater than at 77° longitude, while the ethane mole fraction is 40% enhanced. Throughout the region 227°–298° longitude, east of the impact site, the continuum is depressed by 40%–90% relative to 77° longitude.

214 Normally, the continuum brightness originates in the cold upper troposphere at around
215 200 mbar due to H_2-H_2 translational/rotational collision-induced opacity in Jupiter's hydrogen-
216 dominated atmosphere [Trafton, 1964]. We model the continuum using calculations from
217 Borysow et al., [1985] and fit the measured continuum as it deviates from the calculation.
218 Because features in the spectra are fully-resolved, the measurement of continuum level is
219 independent of degeneracy between continuum emission and gas concentration faced by low-
220 resolution and imaging techniques. No significant deviation is found for the spectra far from the
221 impact site (77° and 125° longitude). The significant deviations of continuum brightness in
222 spectra closer to the impact site must be due to opacity above and interfering with the continuum
223 brightness originating in the upper troposphere. The continuum measurements are consistent
224 with additional opacity introduced at various altitudes and corresponding temperature in the
225 stratosphere.
226 For the spectra at 312° and 324° longitude, the enhanced continuum can be modeled by
227 introducing a surface of infinite opacity in the stratosphere where the physical temperature is
228 equal to the continuum brightness temperature and greater than in the upper tropospheric region
229 in which H_2-H_2 opacity dominates. This sets a lower limit on the altitude at the top of the impact
230 debris at this place and time. A surface at the 60 mbar level fits the 125K continuum brightness
231 temperature in the spectrum at 312° longitude, while a surface at the 45 mbar level fits the
232 warmer 130 K continuum brightness temperature in the spectrum at 324° longitude. The fit to the
233 measured spectra is consistent with narrow line wings due to an opaque layer cutting off the
234 contribution of ethane in the lower stratosphere, at greater pressure where broad line wings are
235 formed.
236 The reduced continuum brightness temperature east of the impact site can be modeled by

237 opacity above the altitude of H_2-H_2 opacity and at colder temperatures. Opacity at the cold
238 tropopause, ~100 mbar, results in a depressed model continuum similar to the retrievals.
239
240 3. DISCUSSION AND CONCLUSIONS
241 The retrieved stratospheric ethane mole fraction is greatest near the impact site (Fig. 3),
242 on the order of 60% enhanced relative to the unperturbed stratosphere (Table 1). Fletcher et al.
243 [2010*a*] retrieve elevated ethane abundance at 304° longitude on July 26 (one week post-impact)
244 relative to August 13 (factor of 1.7-3.2 at 6 mbar). If we apply their relative factor to our August
245 11 measurement of 4.5±0.4 ppmv of ethane at a few mbar at 312°±12° longitude (Table 1), this
246 results in an ethane abundance of 7.6-14.4 ppmv one week after impact compared to the
247 quiescent value of 2.8 ppmv measured by heterodyne spectroscopy [Kostiuk et al., 1987, 1989;
248 Livengood et al., 1993] and confirmed by measurements well away from the impact region.
249 Ethane plausibly could have been formed by fast processes, such as thermochemistry from the
250 direct impact or from the exothermic re-entry of plume ejecta [Harrington and Deming, 2001;
251 Zahnle and Mac Low, 1995; Zahnle, 1996; Livengood et al., 1995, 1997], or perhaps by surface-
252 catalyzed chemistry on injected aerosols. Kostiuk et al. [1996] made limited measurements of
253 ethane eight days after and 15° in longitude away from the SL9 Q1 impact region using IR
254 heterodyne spectroscopy and did not report enhancement of ethane. Fletcher et al. [2010*a*] and
255 Orton et al. [2010] argue, based on Zahnle [1996], that excess ethane will form only in the
256 absence of oxygen-bearing species, from which they conclude the 2009 impactor may have been
257 oxygen-poor, suggesting that it may have been an asteroid, not a comet.
258 Enhanced continuum brightness west of the impact site can be modeled by introducing an
259 infinite opacity layer at the ~45-60 mbar level, an upper limit on the pressure and therefore a

lower limit on the altitude of the top of the aerosol ejecta cloud that likely forms the opacity in Jupiter's atmosphere in the vicinity of the impact site. If the total opacity is finite, then the aerosol cloud must extend to greater temperature and thus higher altitude, to produce the same continuum brightness. This is consistent with de Pater et al. [2010] and Orton et al. [2010] who report deposited particles around 10 mbar and down to the 200-300 mbar level and Fletcher et al. [2010*b*] who report particulates between 3 and 30 mbar less than one week after the impact. West et al. [1995] used HST imaging and aerosol microphysical modeling to estimate particle coagulation and sedimentation times in the SL9 impact regions. They predicted significant settling of ~0.5 μm particles down to the 10 mbar level by one month after impact. Hammel et al. [2010] interpret their results as consistent with a more rapid settling of particles from HST observations of the 2009 impact region compared to HST observations of SL9. Our results imply a settling rate of particles that contribute to the 11.7 μm opacity that is not inconsistent with the West et al. model based on SL9 aerosol altitudes. Although the entry angle of the 2009 impactor was shallower than that of the SL9 fragments [Sanchez-Lavega et al., 2010], the initial altitude of the resulting aerosol cloud might have been similar since it must have originated from the ballistic re-entry from above of ejected plume material, as with SL9, in order to account for the observed angular extent in the day after impact.

Continuum brightness east of the impact site, at 227° to 298° longitude, is reduced to less than that of the unperturbed atmosphere. This can be modeled as a layer of infinite opacity near the tropopause. Uncertainty limits in retrieving the most depressed continuum brightness are consistent with a layer of unit emissivity in equilibrium with a tropopause temperature no more than 5 K cooler than the 110 K tropopause in the *Voyager* profile [e.g., Hanel et al., 1979, Simon-Miller et al., 2006]. It is unclear why the coolest retrieved brightness temperatures at

227° and 245° longitude, ~100±5K, are less than the nominal tropopause temperature of ~110 K. The persistence of sub-micron particles above the cloud deck for weeks after the SL9 impacts was confirmed by West et al. [1995] using *Hubble Space Telescope* (HST) imaging. For an optically thick layer with an appropriate combination of particle size and refractive index at 11.7 μm wavelength, resulting in a particle absorption cross section less than the geometric cross section, the brightness temperature will be less than the physical temperature [Mishchenko et al., 2002]. A detailed test of these ideas is outside the scope of the present work and may be addressed in the future.

The zonal extent of the region of depressed continuum implies the transport of perturbed atmosphere to a longitude offset of 78° east of the impact site, consistent with prograde transport at an average speed of at least 21-28 m/s. The next further east spectrum, at ~125° longitude, is approximately quiescent and limits the maximum prograde wind speed to less than 63 m/s. Enhanced continuum in spectra just west of the impact site could be due to westward transport at higher (warmer) stratospheric altitudes or perhaps direct emplacement of material by the impact. There is not enough sampling in this direction to constrain the extent of impact effects west of the impact site. Flasar et al. [2004] estimated stratospheric wind speeds on Jupiter from *Cassini* CIRS thermal maps, finding an eastward zonal flow in the lower stratosphere of 20–40 m/s, consistent with our results. These velocities are significantly greater than those obtained at this latitude by Porco et al. [2003] from *Cassini* visible imaging of upper tropospheric clouds, confirming that the material sensed in our observations is located in the stratosphere. HST imaging by Hammel et al. [2010] retrieves a maximum eastward velocity of ~10 m/s, in the same direction as our measurements, although a lesser speed. They also measure some of the impact debris traveling westward with a maximum speed of ~5 m/s. Imaging by the amateur astronomy

306 community [Hueso et al., 2010*a*] also is consistent with primarily eastward transport at velocities
307 consistent with the cloud tops. The eastward extent of the debris field measured by HIPWAC is
308 greater than the extent evident in corresponding HST images [Hammel et al., 2010]. The
309 apparent inconsistency could be due to insufficient contrast in the images leading to a lower limit
310 on the extent of the debris field, aerosol evolution and vertical differentiation of particle size
311 populations leading to differential transport in the vertically-varying Jovian wind field, the
312 sensitivities of the employed wavelengths to aerosol populations, or a combination. This
313 suggests that the aerosol properties as well as the vertical distribution of ejecta material and
314 winds remain to be investigated in greater detail.

315 The July 2009 event provided an unexpected second chance to study impact effects on
316 Jupiter, almost exactly 15 years after the SL9 impacts. The subsequent imaging of smaller
317 impact events on Jupiter by A. Wesley and C. Go on 3 June 2010 and by M. Tachikawa and A.
318 Kazuo on 20 August 2010 indicate that impact events are not so rare as once thought.
319 Investigated Jupiter impacts now range from the 2010 fireball events with no detectable after-
320 effects [Hueso et al., 2010*b*] to the chemistry-altering SL9 and 2009 impacts, and continued
321 monitoring and study will further enhance our understanding of the effects of impacts on
322 planetary atmospheres.

323

324 ACKNOWLEDGEMENTS

325 The authors thank Dr. Alan Tokunaga and the staff of the NASA Infrared Telescope Facility for
326 their support of HIPWAC observations of Jupiter, and Drs. Conor Nixon, Carey Lisse, and
327 Michael Mishchenko for valuable discussion. This work was supported by the NASA Planetary
328 Astronomy Program.

329

330 REFERENCES

331 Atakan, A. K., Blass, W. E., Brault, J. W., Daunt, S. J., Halsey, G. W., Jenning, D. E., Reuter, D.
332 C., and Susskind, J., 1983. The 12 Micron Band of Ethane: A Spectral Catalog from 765 cm-
333 l-900 cm-I. NASA/GSFC Technical Memorandum 85108.
334 http://purl.access.gpo.gov/GPO/LPS101012.

335 Bézard, B., 1997. Long-term response of Jupiter's thermal structure to the SL9 impacts. Planet.
336 Space Sci. 45, 1251-1270, doi:10.1016/S0032-0633(97)00068-8.

337 Bjoraker, G. L., Stolovy, S. R., Herter, T. L., Gull, G. E., and Pirger B. E.,1996. Detection of
338 water after the collision of fragments G and K of comet Shoemaker-Levy 9 with Jupiter.
339 Icarus 121, 411-421, doi:10.1006/icar.1996.0096.

340 Borysow, J., Trafton, L., Frommhold, L., and Birnbaum, G., 1985. Modeling of pressure-induced
341 far-infrared absorption spectra: Molecular hydrogen pairs. Astroph. J., 296, 644-654,
342 doi:10.1086/163482.

343 Daunt, S. J., Atakan, A. K., Blass, W. E., Halsey, G. W., Jennings, D. E., Reuter, D. C.,
344 Susskind, J., and Brault, J. W., 1984. The 12 micron band of ethane: High-resolution
345 laboratory analysis with candidate lines for infrared heterodyne searches. Astroph. J., 280,
346 921-936, doi:10.1086/162068.

347 Deming, D., Reuter, D., Jennings, D., Bjoraker, G., McCabe, G., Fast, K., and Wiedemann, G.,
348 1997. Observations and Analysis of Longitudinal Thermal Waves on Jupiter. Icarus 126,
349 301-312, doi:10.1006/icar.1996.5658.

350 Fast, K., Kostiuk, T., Romani, P., Espenak, F., Hewagama, T., Betz, A., Boreiko, R., Livengood
351 T., 2002. Temporal behavior of stratospheric ammonia abundance and temperature following
352 the SL9 impacts. Icarus, 156, 485-497, doi:10.1006/icar.2001.6804.

353 Flasar, F. M., and 39 colleagues 2004. An intense stratospheric jet on Jupiter. Nature 427, 132-
354 135, doi:10.1038/nature02142.4.
355 Fletcher, L. N., Orton, G.S., de Pater, I., Edwards, M.L., Yanamandra-Fisher, P.A., Hammel,
356 H.B., Lisse, C.M., and Fisher, B.M. 2010*b*. The aftermath of the July 2009 impact on Jupiter:
357 Ammonia, temperatures and particulates from Gemini thermal infrared spectroscopy. Icarus
358 211, 568-586, doi:10.1016/j.icarus.2010.09.012.
359 Fletcher, L. N., Orton, G.S., de Pater, I., Mousis, O., 2010*a*. Jupiter's stratospheric hydrocarbons
360 and temperatures after the July 2009 impact from VLT infrared spectroscopy, A&A 524,
361 A46, doi:10.1051/0004-6361/201015464.
362 Griffith, C. A., Bézard, B., Greathouse, T. K., Kelly, D. M., Lacy, J. H., and Noll, K. S., 1997.
363 Thermal infrared imaging spectroscopy of Shoemaker-Levy 9 impact sites: Spatial and
364 vertical distributions of NH_3, C_2H_4, and 10-μm dust emission. Icarus 128, 275-293,
365 doi:10.1006/icar.1997.5752.
366 Harrington, J., and Deming D. 2001. Models of the Shoemaker-Levy 9 impacts. I. Ballistic
367 Monte Carlo plume. Astroph. J. 561, 455-467, doi:10.1086/323210.
368 Harrington, J., de Pater, I., Brecht, S. H., Deming, D., Meadows, V., Zahnle, K., and Nicholson,
369 P. D. 2004. Lessons from Shoemaker-Levy 9 about Jupiter and planetary impacts. In:
370 Bagenal, R., Dowling, T., McKinnon, W. (Eds.), Jupiter. The Planet, Satellites and
371 Magnetosphere, Cambridge University Press, Cambridge, pp. 159-184.
372 Hammel, H. B., and 11 colleagues 2010. Jupiter after the 2009 impact: *Hubble Space Telescope*
373 imaging of the impact-generated debris and its temporal evolution, Astroph. J. 715, L150-
374 L154, doi:10.1088/2041-8205/715/2/L150
375 Hanel, R. A., and 12 colleagues 1979. Infrared observations of the Jovian system from *Voyager*

376 *1*. Science 204, 972-976.
377 Hewagama, T., Goldstein, J., Livengood, T., Buhl, D., Espenak, F., Fast, K., Kostiuk, Th., and
378 Schmülling, F., 2008. Beam integrated high-resolution infrared spectra: Accurate modeling
379 of thermal emission from extended clear atmospheres. J. Quant. Spectrosc. Radiat. Trans.
380 109, 1081-1097, doi:10.1016/j.jqsrt.2007.12.022.
381 Hueso, R., Legarreta, J., Pérez-Hoyos, S., Rojas, J. F., Sánchez-Lavega, A., and Morgado, A.
382 2010*a*. The international outer planets watch atmospheres node database of giant-planet
383 images. Planet. Space Sci. 58, 1152-1159. doi:10.1016/j.pss.2010.04.006.
384 Hueso, R., and 16 colleagues 2010*b*. First Earth-based detection of a superbolide on Jupiter.
385 Astroph. J. 721, L129-L133. doi:10.1088/2041-8205/721/2/L129.
386 Kim, S. J., Caldwell, J., Rivolo, A. R., Wagener, R., and Orton G. S., 1985. Infrared polar
387 brightening on Jupiter: III. Spectrometry from the *Voyager 1* IRIS experiment. Icarus 64,
388 233-248, doi:10.1016/0019-1035(85)90088-0.
389 Kostiuk, T., and Mumma, M. J., 1983. Remote sensing by IR heterodyne spectroscopy, Appl.
390 Opt. 22, 2644-2654, doi:10.1364/AO.22.002644.
391 Kostiuk, T., Espenak, F., Mumma, M. J., Deming, D., and Zipoy D., 1987. Variability of ethane
392 on Jupiter. Icarus 72, 394-410, doi:10.1016/0019-1035(87)90182-5.
393 Kostiuk, T., Espenak, F., Mumma, M. J., and Romani P., 1989. Infrared studies of hydrocarbons
394 on Jupiter. Infrared Phys. Technol. 29, 199-204, doi:10.1016/0020-0891(89)90048-1.
395 Kostiuk, T., 1994. Physics and chemistry of upper atmospheres of planets from infrared
396 observations. Infrared Phys. Technol. 35(2), 243-266, doi:10.1016/1350-4495(94)90084-1.
397 Kostiuk, T., Buhl, D., Espenak, F., Romani, P., Bjoraker, G., Fast, K., Livengood, T., and Zipoy
398 D., 1996. Stratospheric ammonia on Jupiter after the SL9 collision. Icarus 121, 431-441,

399 doi:10.1006/icar.1996.0098.
400 Lellouch, E., and 13 colleagues, 1995. Chemical and thermal response of Jupiter's atmosphere
401 following the impact of comet Shoemaker–Levy 9. Nature 373, 592-595,
402 doi:10.1038/373592a0.
403 Livengood, T. A., Kostiuk, T., Espenak, F., and Goldstein, J. J., 1993. Temperature and
404 Abundances in the Jovian Auroral Stratosphere 1. Ethane as a Probe of the Millibar Region.
405 J. Geophys. Res. 98(E10), 18813-18821, doi:10.1029/93JE01043.
406 Livengood, T. A., Käufl, H. U., Kostiuk, T., Bjoraker, G. L., Romani, P. N., Wiedemann, G.,
407 Mosser, B., and Sauvage M., 1995. Multi-wavelength thermal-infrared imaging of SL9
408 impact phenomena. European Southern Observatory Astrophysics Symposia 52, 137-145.
409 Livengood, T. A., Kostiuk, T., and Käufl, H. U. 1997. Smoke gets in your eyes: Thermal
410 emission from the SL9 stratospheric debris fields, Bull. Am. Astron. Soc. 29, 1008 (abstract).
411 Mishchenko, M. I., Travis, L. D., and Lacis, A. A., 2002. Scattering, Absorption, and Emission
412 of Light by Small Particles, Cambridge University Press.
413 Nixon, C. A., and 14 colleagues 2007. Meridional variations of C2H2 and C2H6 in Jupiter's
414 atmosphere from *Cassini* CIRS infrared spectra. Icarus 188, 47-71,
415 doi:10.1016/j.icarus.2006.11.016.
416 Orton, G., and 57 colleagues 1995. Collision of comet Shoemaker-Levy 9 with Jupiter observed
417 by the NASA Infrared Telescope Facility, Science 267, 1277-1288,
418 doi:10.1126/science.7871423.
419 Orton, G.S., and 26 colleagues 2010. The atmospheric influence, size and possible asteroidal
420 nature of the July 2009 Jupiter impactor. Icarus 211, 587-682,
421 doi:10.1016/j.icarus.2010.10.010.

de Pater, I., Fletcher, L. N., Pérez-Hoyos, S., Hammel, H. B., Orton, G. S., Wong, M. H., Luszcz-Cook, S., Sánchez-Lavega, A., and Boslough, M., 2010. A multi-wavelength study of the 2009 impact on Jupiter: Comparison of high resolution images from Gemini, Keck and HST. Icarus 210, 722-741. doi:10.1016/j.icarus.2010.07.010.

Porco, C. C., and 23 colleagues, 2003. Cassini imaging of Jupiter's atmosphere, satellites, and rings. Science, 299, 1541-1547, doi:10.1126/science.1079462.

Russell, C. T., and Dougherty, M. K. 2010. Magnetic Fields of the Outer Planets. Space Sci. Rev. 152, 251-269, doi: 10.1007/s11214-009-9621-7.

Sánchez-Lavega, A., and 15 colleagues 2010. The Impact of a large object on Jupiter in 2009 July. Astroph. J. 715, L155-L159. doi:10.1088/2041-8205/715/2/L155.

Simon-Miller, A. A., Conrath, B. J., Gierasch, P. J., Orton, G. S., Achterberg, R. K., Flasar, F. M., and Fisher, B. M., 2006. Jupiter's atmospheric temperatures: From *Voyager* IRIS to *Cassini* CIRS. Icarus, 180, 98-112, doi:10.1016/j.icarus.2005.07.019.

Trafton, L. M., 1964. The thermal opacity in the major planets, Astroph. J., 140, 1340-1341, 10.1086/148039.

Vander Auwera, J., Moazzen-Ahmadi, N., Flaud, J.-M., 2007. Towards an accurate database for the 12 mm region of the ethane spectrum. Astrophys. J. 662, 750–757, doi:10.1086/515567.

West, R. A., Karkoschka, E., Friedson, A. J., Seymour, M., Baines, K. H., and Hammel H. B., 1995. Impact debris particles in Jupiter's stratosphere. Science 267, 1296-1301, doi:10.1126/science.7871426.

Zahnle, K., 1996. Dynamics and chemistry of SL9 plumes. In: Noll, K. S., Weaver, H. A., Feldman, P. D. (Eds.), The Collision of Comet Shoemaker-Levy 9 and Jupiter. Cambridge University Press, Cambridge, pp. 183–212.

445 Zahnle, K., and Mac Low, M.-M., 1995. A simple model for the light curve generated by a
446 Shoemaker-Levy 9 impact. J. Geophys. Res. 100(E8), 16885-16894, doi:10.1029/95JE01620.
447

448 FIGURE CAPTIONS

449

450

451 Fig. 1. HIPWAC spectra, near (312° longitude, *left*) and far from (77° longitude, *right*) the 2009
452 July impact site, 11–12 August 2009 (histograms, smoothed for clarity). The solid curve is a
453 model emergent spectrum for ethane in Jupiter's stratosphere. Vertical lines represent logarithm
454 of C_2H_6 line strength at 180 K. The frequency scale is the difference from the $^{14}CO_2$ laser local
455 oscillator frequency at 851.4895 cm^{-1}. Prominent features at ~150 MHz and ~1300 MHz are not
456 due to C_2H_6 and are unidentified; they are masked from the retrievals. The horizontal dotted line
457 is a fitted continuum. The dashed-line curve is a model for the quiescent stratosphere (2.8 ppmv
458 C_2H_6).

459

460 Fig. 2. Variation of ethane peak emission measured by HIPWAC at 56°S latitude on Jupiter on
461 the central meridian on 2009 August 11 UT. Central meridian longitude (CML) is noted for each
462 panel, 227° through 324° System III, and each spectrum covers 10°-20° in longitude. The
463 modeled emergent spectrum fitted to the measured data (histograms) is shown by a smooth
464 curve; horizontal dotted lines indicate retrieved continuum. The combination of pressure-
465 sensitive line shape and absolute radiance across the full bandpass simultaneously constrains the
466 C_2H_6 mole fraction and the altitude of an idealized opaque surface (representing a lower altitude
467 limit on the top of the impact debris) in the temperature-pressure profile for each spectrum. This
468 is reflected in the broadening (227°–298° CML) or narrowing (312°–324° CML) of the line
469 wings.

470

471 Fig. 3. Variation of retrieved ethane mole fraction (*upper*) and continuum brightness (*lower*)
472 from spectra acquired at 56°S latitude on 2009 August 11 and 12 UT. Dotted lines enclose the
473 range of C_2H_6 mole fraction determined previously from heterodyne spectroscopy of the
474 quiescent stratosphere [*Kostiuk et al.*, 1987]. Retrieved C_2H_6 mole fraction is greatest near the
475 impact longitude of 305° (dashed line). Retrieved continuum brightness is greatest near the
476 impact site and can be modeled by opacity in the stratosphere. Depressed continuum brightness
477 toward planetary east of the impact can be modeled by opacity near the cold tropopause. No
478 measurements were made in the interval 125°–227° longitude.

479

480 TABLE

481

482 **Table 1: Variation with longitude of extracted spectroscopic parameters**[a]

UT Date 2009	UT	Longitude[b] Sys III	Fitted C_2H_6 mole fraction[c]	Fitted continuum[d]	Relative C_2H_6 mole fraction[e]	Relative continuum[f]
Aug-12	09:17:41	77°±6°	2.9±0.4	0.34±0.04	-	-
Aug-11	14:44:43	125°±5°	3.6±0.7	0.36±0.06	1.3±0.3	1.0±0.2
Aug-11	07:39:22	227°±14°	2.5±0.3	0.05±0.04	0.9±0.2	0.1±0.1
Aug-11	08:04:53	243°±12°	2.6±0.3	0.07±0.04	0.9±0.2	0.2±0.1
Aug-11	08:25:17	255°±11°	3.3±0.4	0.20±0.04	1.1±0.2	0.6±0.1
Aug-11	08:49:31	270°±14°	3.5±0.4	0.21±0.04	1.2±0.2	0.6±0.1
Aug-11	09:14:47	285°±12°	3.1±0.3	0.10±0.04	1.1±0.2	0.3±0.1
Aug-11	09:36:36	298°±12°	3.4±0.3	0.11±0.04	1.2±0.2	0.3±0.1
2009-Jul-19		305°	*Impact site, at 56° S latitude (planetocentric).*			
Aug-11	09:58:48	312°±12°	4.5±0.4	0.47±0.03	1.6±0.3	1.4±0.2
Aug-11	10:20:03	324°±11°	3.9±0.3	0.56±0.03	1.4±0.2	1.6±0.2

483 *a* Contribution to ethane emission features originates between 0.2 and 20 mbar, with maximum
484 contribution around a few mbar.
485 *b* Jupiter System III longitude, (radio-magnetic coordinates; Russell and Dougherty 2010),
486 indicating range of longitude during integration. Spectra acquired on central meridian at the
487 56° south impact latitude (planetocentric).
488 *c* Retrieved ethane (C_2H_6) mole fraction in parts per million by volume (ppmv) from radiative
489 transfer analysis.
490 *d* Retrieved thermal continuum brightness, units of erg/cm^2/s/sr/cm^{-1} from radiative transfer
491 analysis.
492 *e* Ethane mole fraction normalized to retrieval at 77° longitude.
493 *f* Continuum brightness normalized to retrieval at 77° longitude.